Nano Energy (2015) 13, 355–367

Available online at www.sciencedirect.com

ScienceDirect

journal homepage: www.elsevier.com/locate/nanoenergy

RAPID COMMUNICATION

Enhancement of thermoelectric performance in n-type $PbTe_{1-y}Se_y$ by doping Cr and tuning Te:Se ratio

Eyob K. Chere[a,1], Qian Zhang[a,1], Kenneth McEnaney[b], Mengliang Yao[c], Feng Cao[a], Jingying Sun[a], Shuo Chen[a], Cyril Opeil[c], Gang Chen[b], Zhifeng Ren[a,*]

[a]Department of Physics and TcSUH, University of Houston, Houston, TX 77204, USA
[b]Department of Mechanical Engineering, Massachusetts Institute of Technology, Cambridge, MA 02139, USA
[c]Department of Physics, Boston College, Chestnut Hill, MA 02467, USA

Received 2 December 2014; received in revised form 2 February 2015; accepted 17 February 2015
Available online 26 February 2015

KEYWORDS
Thermoelectric;
Cr doping;
Te:Se ratio;
Average *ZT*;
Efficiency

Abstract
Lead telluride and its alloys have been extensively studied for medium temperature thermoelectric applications due to decent figure-of-merit (*ZT*) at temperature close to 900 K. However, little emphasis has been given to improve the *ZT* near room temperature. In this investigation, we report a systematic study of Cr doping in $PbTe_{1-y}Se_y$ with y=0, 0.25, 0.5, 0.75, 0.85, and 1. We found the peak *ZT* temperature increased with increasing concentration of Se. The highest *ZT* of ~0.6 at room temperature in Te-rich $Cr_{0.015}Pb_{0.985}Te_{0.75}Se_{0.25}$ was obtained due to a lowered thermal conductivity and enhanced power factor resulted from high Seebeck coefficient of about $-220\ \mu V\ K^{-1}$ and high Hall mobility ~1120 $cm^2\ V^{-1}\ s^{-1}$ at room temperature. A room temperature *ZT* of ~0.5 and peak *ZT* of ~1 at about 573–673 K is shown by Se-rich sample $Cr_{0.01}Pb_{0.99}Te_{0.25}Se_{0.75}$. This improvement of the room temperature *ZT* improved the average *ZT* over a wide temperature range and could potentially lead to a single leg efficiency of thermoelectric conversion for Te-rich $Cr_{0.015}Pb_{0.985}Te_{0.75}Se_{0.25}$ up to ~11% and Se-rich $Cr_{0.01}Pb_{0.99}Te_{0.25}Se_{0.75}$ up to ~13% with cold side and hot side temperature at 300 K and 873 K, respectively, if matched with appropriate p-type legs.

*Corresponding author.
Tel.: +1 713 743 8217; fax: +1 713 743 8201.
E-mail address: zren@uh.edu (Z. Ren).
[1]Equal contributor.

http://dx.doi.org/10.1016/j.nanoen.2015.02.026
2211-2855/

Introduction

Thermoelectric materials can directly convert heat into electricity without moving parts [1,2]. The performance of a thermoelectric material is characterized by its dimensionless figure of merit (ZT), which is a function of materials' temperature-dependent properties [1,3], $ZT = [S^2\sigma/(\kappa_e+\kappa_L)]T$, where S, σ, κ_e, κ_L, and T are the Seebeck coefficient, electrical conductivity, electronic thermal conductivity, lattice thermal conductivity, and absolute temperature, respectively [3,4]. Accordingly, making an efficient thermoelectric generator requires maximizing ZT over a wide temperature range, which ultimately demands materials with high Seebeck coefficients, high electrical conductivities, and low thermal conductivities. It is very difficult to independently tune these parameters since they are interrelated. Significant efforts have been put into decoupling them using various techniques [5,6]. The introduction of nanostructures into bulk thermoelectric materials gives the opportunity to independently tune these parameters [7,8] and significantly reduces the thermal conductivity by scattering a broad spectrum of phonons [9,10]. Recently, band engineering based on modifying the band structure by alloying [11–13] or doping to create impurity levels for resonating with the host band [14,15] or both [16,17] lead to significant achievements in obtaining higher ZT values.

Lead telluride (PbTe) [18] with its intrinsically low thermal conductivity [19] is one of the most studied thermoelectric materials for medium temperature applications [20]. The thermoelectric performance of PbTe has been enhanced by alloying with its isostructural sister compound PbSe. The partial substitution of Te by Se leads to disorder via atomic mass fluctuations, distortion in the crystal lattice and formation of defect states, which can effectively scatter phonons more than charge carriers (electrons or holes) to reduce thermal conductivity [9,10,21]. Significant progress has been reported in improving the ZT of PbTe by simultaneous alloying, doping, and band engineering. Tl acts as a resonant dopant in PbTe to enhance the ZT to $\sim$1.5 by modifying the band structure [14]. By potassium doping, a peak ZT value of $\sim$1.7 at 873 K was achieved in $K_{0.02}Pb_{0.98}Te_{0.15}Se_{0.85}$ [20]. A ZT of $\sim$1.8 was obtained in p-type $Na_{0.02}Pb_{0.98}Te_{0.85}Se_{0.15}$ by band convergence [11]. Even though the peak ZTs of these materials at high temperatures are high, the average ZTs are low because the ZTs below 400 K are very low [22,23], which significantly reduces the efficiency of these materials.

Cr was reported as a resonant donor in PbTe, PbSe, and $PbTe_{1-y}Se_y$ systems at low temperatures [24]. The room-temperature Seebeck coefficient and power factor in PbTe [25] and PbSe [26] can be increased by Cr doping. However, the improvement was proved to not be due to resonant scattering. One study shows the formation of a Cr resonant state in PbTe, with energy 100 meV above the conduction band bottom of PbTe at 0 K, but the state moves into the band gap when the temperature increases to room temperature and hence does not contribute to a power factor enhancement at or above room temperature [27]. Another study also found Cr impurity states within the conduction band of PbTe [25]. However, the band distortion that comes from such a resonance of the Cr impurity level is not broadened well enough to properly align the Fermi level with the enhanced density of states and hence does not contribute to the enhancement of Seebeck coefficient.

In this work, we systematically studied the enhancement of both the ZT near room temperature and the average ZT of $PbTe_{1-y}Se_y$ across a wide temperature range with $y = 0$, 0.25, 0.50, 0.75, 0.85, and 1 by Cr doping. The reduction in thermal conductivity due to phonon scattering by the introduced point defects from the alloying, together with the optimized electronic properties by Cr doping, contributed to the enhancement of the room temperature ZT to $\sim$0.6 for Te-rich $Cr_{0.015}Pb_{0.985}Te_{0.75}Se_{0.25}$ and a peak ZT of $\sim$1 at about 573 K to 673 K for Se-rich $Cr_{0.01}Pb_{0.99}Te_{0.25}Se_{0.75}$ with a room temperature ZT of $\sim$0.5. The calculated efficiency of each single leg $Cr_{0.015}Pb_{0.985}Te_{0.75}Se_{0.25}$ and $Cr_{0.01}Pb_{0.99}Te_{0.25}Se_{0.75}$ is $\sim$11% and $\sim$13%, respectively, with a cold side temperature at 300 K and hot side temperature at 873 K.

Experimental section

Synthesis

Cylindrical shaped ingots of $\sim$10 g $Cr_xPb_{1-x}Te_{1-y}Se_y$ (x = 0.005, 0.01, 0.015, and 0.02, and y = 0, 0.25, 0.50, 0.75, 0.85, and 1) were prepared in a carbon coated quartz tube by using high purity elements (Cr pieces, 99.99%; Pb granules, 99.99%; Te chunks 99.999%; and Se granules, 99.99%) according to their stoichiometric weights. The tubes were evacuated to $\sim 3\times10^{-4}$ Pa and sealed, and then slowly heated at 1000–1100 °C at a rate of 200 °C/h and then held at that temperature for 6 h, then slowly cooled at the same rate to 650 °C and kept there for 50 h, and then finally cooled to room temperature. The ingots obtained from this procedure were cleaned and hand milled in a glove box with an argon environment. The hand-milled powder was then loaded into a half-inch graphite die, hot pressed at 600 °C for 2 min, air cooled, polished to disks with average thickness of 1.8–2 mm. These disks are cut into desired shapes for further characterizations.

Characterizations

X-ray diffraction spectra analysis was conducted on a PANalytical multipurpose diffractometer with an X'celerator detector (PANalytical X'Pert Pro). The microstructures were investigated by a scanning electron microscope (SEM, LEO 1525) and a high resolution transmission electron microscope (HRTEM, JEOL 2100F). The chemical composition was analyzed on an energy-dispersive X-ray (EDX) spectrometer attached to SEM (JEOL 6330F). The thermal diffusivity (α) was measured by a laser flash analyzer (Netzsch LFA 457) on a half-inch disk with thickness of 1.8–2 mm, the specific heat (C_p) was measured by a differential scanning calorimetry thermal analyzer (Netzsch DSC 404C) on a smaller disk with diameter of 6 mm and thickness less than 0.8 mm and the volumetric density (D) was measured by the Archimedes method. The total thermal conductivity was calculated by $\kappa = D\alpha C_p$. We cut a bar of $\sim$10 mm × 2 mm × 2 mm from the half-inch disc for Seebeck coefficient (S) and electrical conductivity (σ) measurements. The Seebeck coefficient (S) and electrical conductivity (σ) measurements were done using a static direct current method and a four-point direct current switching method,

respectively, on a commercial (ULVAC ZEM-3) system. The room-temperature Hall coefficient (R_H) was measured using a Quantum Design Physical Properties Measurement System on a bar with dimension of 10 mm × 2 mm × 0.5 mm cutting from the same disc. The Hall carrier concentration n_H and Hall mobility μ_H were calculated from the Hall coefficient R_H by $n_H = (eR_H)^{-1}$ and $\mu_H = \sigma R_H$, respectively. Our measurements are accurate to within 12% for the ZT and 10% for the power factor, coming from a 3% error in electrical conductivity, a 5% error in Seebeck coefficient, and a 7% error in thermal conductivity. Error bars were not used in the figures to increase the readability of the curves.

Results and discussion

The lower thermal conductivity due to large Grüneisen parameter values and nanocomposite microstructures [26,28], and the improved power factor values by Cr doping have improved the average ZT of n-type PbSe over a wide temperature range (300–873 K) [26]. When Cr is doped into PbTe, the room temperature power factor increased dramatically compared with the other n-type PbTe alloys [25]. The best power factor at room temperature is ~36.50 μW cm^{-1} K^{-2} in $Cr_{0.025}Pb_{0.975}Te$, which is approximately a 22% increase compared to Cr-doped PbSe. This result is close to the values reported by Paul et al. [25] on Cr-doped PbTe. However, the thermal conductivity increased to 2.6 W m^{-1} K^{-1} at room temperature and 1.3 W m^{-1} K^{-1} at 773 K, higher than that of Cr-doped PbSe (2.2 W m^{-1} K^{-1} at room temperature and 1.0 W m^{-1} K^{-1} at 773 K). Figure 1 shows the temperature dependence of the thermoelectric properties of Cr-doped PbTe at various Cr concentrations. The calculated ZT is ~0.45 at room temperature and ~0.8 at 600–773 K. The relatively lower thermal conductivity in PbSe and higher room temperature power factor from Cr-doped PbTe motivated us to further optimize the alloy system by achieving the best power factor and lower thermal conductivity to achieve a higher room temperature ZT and average ZT. We used the highest C_p of $Cr_{0.03}Pb_{0.97}Te$ for all samples $Cr_xPb_{1-x}Te$ with various Cr concentrations (Figure 1(e)). For other samples $Cr_xPb_{1-x}Te_{1-y}Se_y$, the selected measured C_ps are shown in Figure 2. The lattice thermal conductivity is obtained by subtracting the electronic thermal conductivity ($\kappa_e = L\sigma T$, where L is the Lorenz number calculated using a two-band Kane model) from the total thermal conductivity.

Samples with compositions $Cr_xPb_{1-x}Te_{0.75}Se_{0.25}$ and $Cr_xPb_{1-x}Te_{0.25}Se_{0.75}$ were prepared and the temperature dependences of the thermoelectric properties are shown in Figures 3 and 4. For $Cr_xPb_{1-x}Te_{0.75}Se_{0.25}$, the Seebeck coefficient shows a slight increase when the Cr doping level

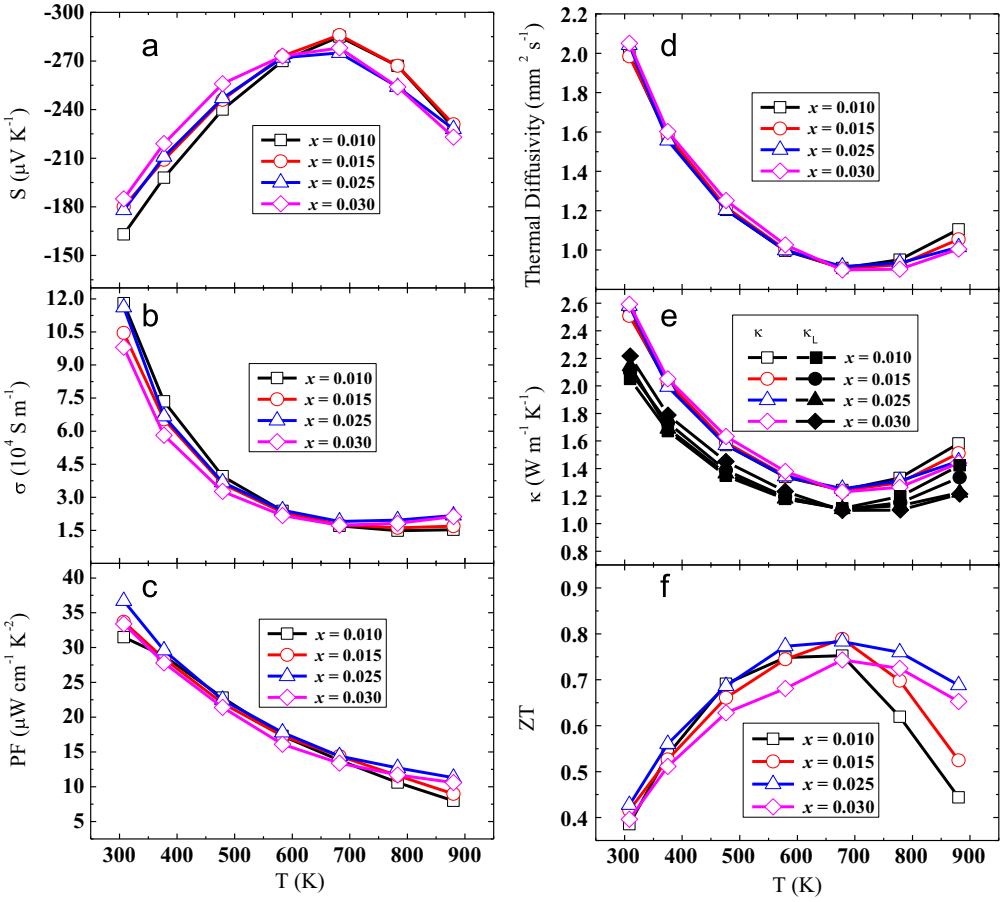

Figure 1 Temperature-dependent thermoelectric properties of $Cr_xPb_{1-x}Te$ at various dopant concentrations (x = 0.01, 0.015, 0.025, and 0.03). (a) Seebeck coefficient, (b) electrical conductivity, (c) power factor, (d) thermal diffusivity, (e) total thermal conductivity and lattice thermal conductivity, and (f) ZT.

increases from 1 atm% to 2 atm% and a strong bipolar effect at above 600 K. The electrical conductivity first increases when the Cr doping reaches a critical value of 1.5 atm% and then decreases when the doping concentration of Cr increases to 2 atm%. This is due to the reduction in the mobility of electrons with increasing defect density as the dopant contributes to disorder at higher concentrations. It shows a relatively higher electrical conductivity at 1.5 atm% Cr doping level, which is attributed to the higher carrier mobility ($\sim$1120 $cm^2 V^{-1} s^{-1}$) as confirmed by the room-temperature Hall measurement. This electrical conductivity in combination with the high Seebeck coefficient yields a higher room-temperature power factor of $\sim$24 $\mu W cm^{-1} K^{-2}$ (Figure 3(c)). The room temperature mobility (1120 $cm^2 V^{-1} s^{-1}$) and power factor ($\sim$24 $\mu W cm^{-1} K^{-2}$) are respectively lower by $\sim$20% and 37% compared to the mobility ($\sim$1404 $cm^2 V^{-1} s^{-1}$) and power factor ($\sim$38 $\mu W cm^{-1} K^{-2}$) of Cr-doped PbTe reported by Paul et al. [25]. However, despite the 37% power factor reduction, the *ZT* value of $Cr_{0.015}Pb_{0.985}Te_{0.75}Se_{0.25}$ is $\sim$66% higher than that of Cr-doped PbTe [25] due to the highly suppressed thermal conductivity. The thermal conductivity is decreased due to the introduced atomic scale defects by alloying via atomic mass disorder, vacancies and dislocations present in the samples as we can see from the HRTEM images in Figure 6(b). The atomic scale defects (atomic mass disorder and vacancies) strongly scatter phonons of high frequency and short mean free path where as the mesoscale defects (grain boundaries and dislocations) scatter phonons of low frequency and long mean free path. From the SEM images (Figure 5) and TEM image (Figure 6(a)), our sample is composed of nano grains of size ranging from 50 nm to several microns, which assist the scattering of phonons of mean free path of the order of greater than or equal to 50 nm and

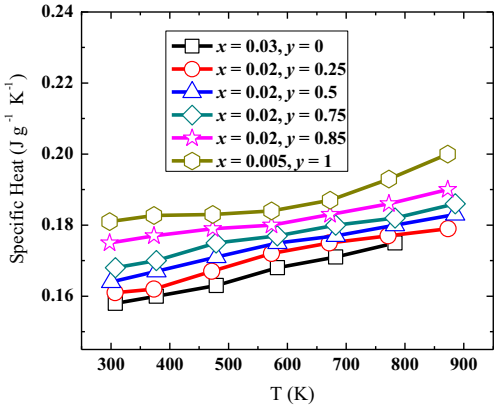

Figure 2 Temperature-dependent specific heat of $Cr_xPb_{1-x}Te_{1-y}Se_y$ (x = 0.005, 0.02, and 0.03, y = 0, 0.25, 0.5, 0.75, 0.85, and 1).

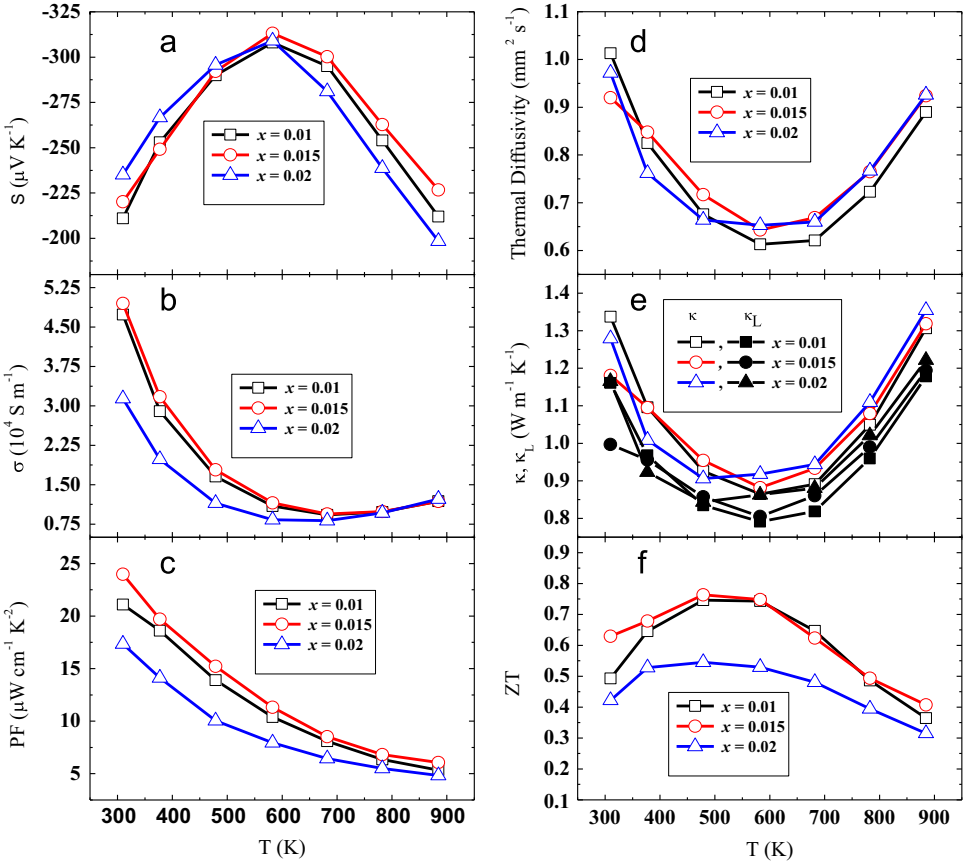

Figure 3 Temperature-dependent thermoelectric properties of $Cr_xPb_{1-x}Te_{0.75}Se_{0.25}$ (x = 0.01, 0.015, and 0.02). (a) Seebeck coefficient, (b) electrical conductivity, (c) power factor, (d) thermal diffusivity, (e) total thermal conductivity and lattice thermal conductivity, and (f) *ZT*.

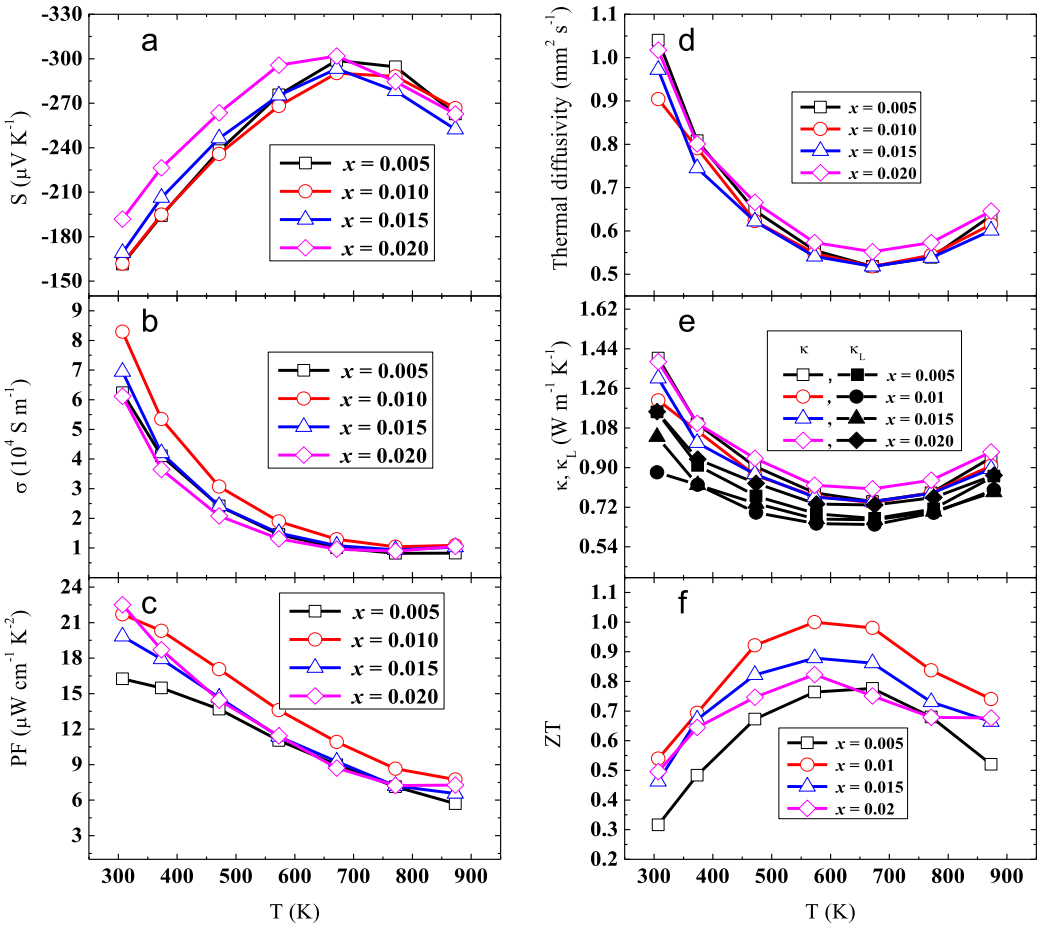

Figure 4 Temperature-dependent thermoelectric properties of $Cr_xPb_{1-x}Te_{0.25}Se_{0.75}$ (x = 0.005, 0.01, 0.015, and 0.02). (a) Seebeck coefficient, (b) electrical conductivity, (c) power factor, (d) thermal diffusivity, (e) total thermal conductivity and lattice thermal conductivity, and (f) *ZT*.

microns. However, it has been proven that in $PbTe_{1-y}Se_y$ alloys most of the thermal conductivity is contributed by phonons of mean free path less than 10 nm. Therefore, a grain size of less than 10 nm is needed to achieve a significant reduction of thermal conductivity by nanostructuring [29]. The lowest thermal conductivity is ~0.9 W m^{-1} K^{-1} at 573 K. However, there is a small influence on the room temperature value with Cr doping. It decreased and then increased when the Cr doping level varied from 1 atm% to 2 atm% showing a minimum value of ~1.2 W m^{-1} K^{-1} at a doping concentration of 1.5 atm%, which leads to a record *ZT* of ~0.6 in lead chalcogenide systems at room temperature. This *ZT* value is not too much lower than the *ZT* of the well-known state-of-the-art n-type room temperature material $Bi_2Te_{2.7}Se_{0.3}$ [30]. The increase of the thermal conductivity at elevated temperatures is clearly due to the minority carriers.

For $Cr_xPb_{1-x}Te_{0.25}Se_{0.75}$, as shown in Figure 4, the Seebeck coefficient shows a similar trend as the Te-rich (Figure 3) system with increasing Cr concentration. However, this composition is less susceptible to bipolar conduction and the bipolar temperature is higher than that of the Te-rich composition. This is due to the suppression of minority carriers by the band gap increase in the Se-rich composition with increasing temperature consistent with the previous studies [31]. The electrical conductivity also follows a similar trend as the Te-rich composition in such a way that it increased when the Cr concentration increased to a critical value of 1.5 atm% then decreased when it exceeds this critical level. The lowest room temperature thermal conductivity is ~1.25 and ~0.8 at about 673 K in $Cr_{0.01}Pb_{0.99}Te_{0.25}Se_{0.75}$, giving rise to a room temperature *ZT* of ~0.5 and the highest peak *ZT* of ~1 at approximately 573 K to 673 K.

We then prepared different samples with different Se concentrations to check the alloying effect. Figure 7 shows the temperature dependence of (a) the Seebeck coefficient, (b) the electrical conductivity, (c) the power factor, (d) the thermal diffusivity, (e) the total thermal conductivity and the lattice thermal conductivity, and (f) the *ZT* with a fixed Cr concentration of 1 atm% and different Se concentrations of y = 0.25, 0.5, 0.75, and 0.85. The electrical conductivity of all the samples decreased with increasing temperature, consistent with the attributes of degenerate semiconductors. At fixed concentration of 1 atm% Cr doping, the room-temperature Seebeck coefficient decreased from −211 μV K^{-1} to −157 μV K^{-1} with increasing Se concentration. The Seebeck coefficient of all the samples decreased at higher temperatures showing a bipolar transport nature and it was found that the temperature at which the bipolar effect becomes important for Te-rich samples is lower than that of Se-rich samples. The

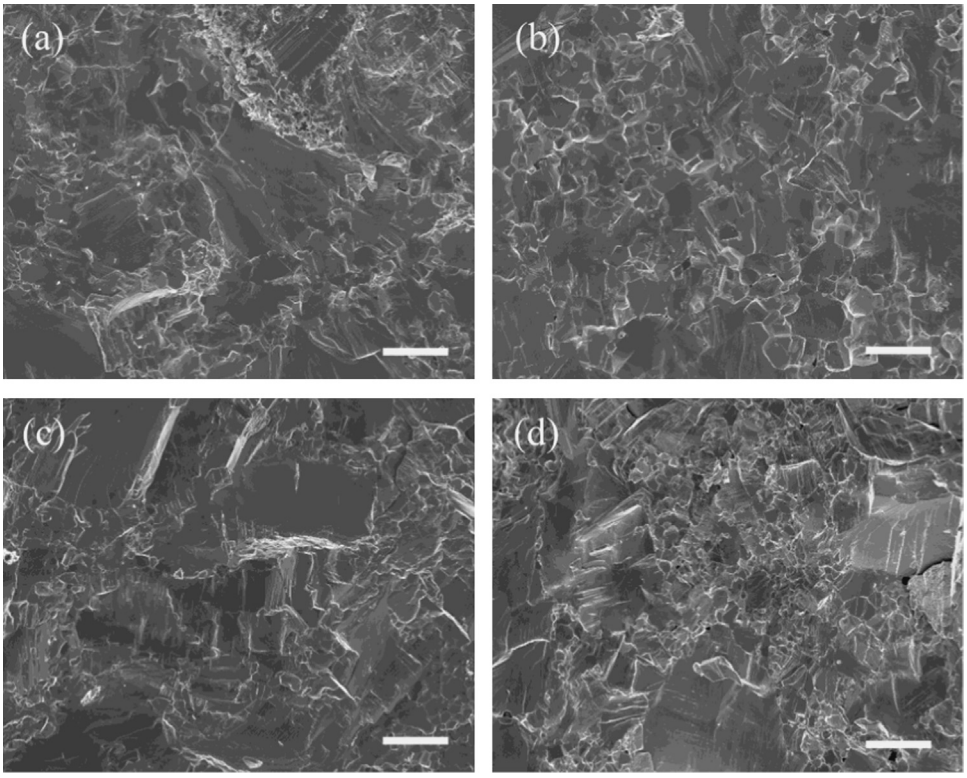

Figure 5 SEM for (a) $Cr_{0.025}Pb_{0.975}Te$, (b) Te-rich $Cr_{0.015}Pb_{0.985}Te_{0.75}Se_{0.25}$, (c) Se-rich $Cr_{0.01}Pb_{0.99}Te_{0.25}Se_{0.75}$, and (d) $Cr_{0.005}Pb_{0.995}Se$. The scale bar is 10 μm.

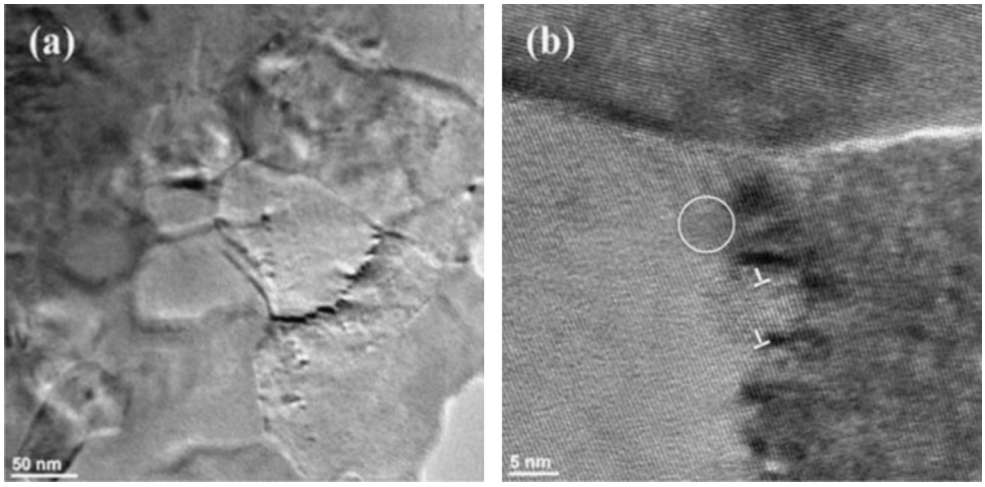

Figure 6 Low magnification TEM image (a), and HRTEM image (b) showing grain boundaries, point defects marked by circles, and thread dislocations marked by ⊥.

electrical conductivity increased when the Se concentration increased to 75 atm% and then decreased above this concentration showing a higher value at an optimum Se concentration of 75 atm%. The high electrical conductivity manifested by the Se-rich sample $Cr_{0.01}Pb_{0.99}Te_{0.25}Se_{0.75}$ resulted in a higher power factor across the whole temperature range. This high electrical conductivity is attributed to the relatively higher carrier concentration ($\sim 8.12 \times 10^{18}$ cm^{-3}) as evidenced by the room-temperature Hall measurement. The thermal conductivity is heavily decreased compared to Cr-doped PbTe and PbSe samples due to phonon scattering by the point defects resulting from alloying. We see a minimum thermal conductivity of ~ 0.8 $W\,m^{-1}\,K^{-1}$ at 573 K in $Cr_{0.01}Pb_{0.99}Te_{0.5}Se_{0.5}$ with equal amount of Te and Se. This is approximately a 72% decrease compared to PbTe for the same Cr doping level of 1 atm%. This reduction is related to the maximum distortion of the crystal lattice due to the maximum entropic atomic mass fluctuation as confirmed by theoretical calculations and experimental studies [21,29]. The increase in thermal conductivity at higher temperatures is due to the contribution of heat transport by minority carriers (holes). The highest *ZT* is ~ 1 at approximately 573 K to 673 K in Se-rich $Cr_{0.01}Pb_{0.99}Te_{0.25}Se_{0.75}$.

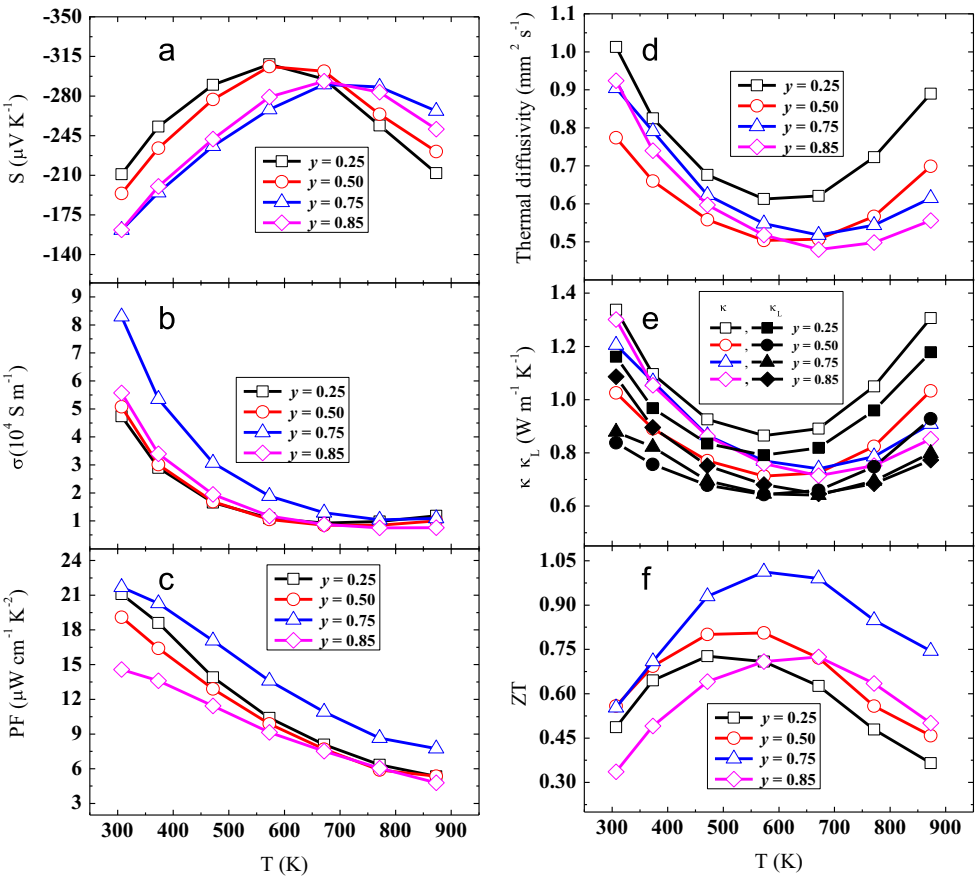

Figure 7 Temperature-dependent thermoelectric properties of $Cr_{0.01}Pb_{0.99}Te_{1-y}Se_y$ (y = 0.25, 0.5, 0.75, and 0.85) with fixed Cr concentration of 1 atm%. (a) Seebeck coefficient, (b) electrical conductivity, (c) power factor, (d) thermal diffusivity, (e) total thermal conductivity and lattice thermal conductivity, and (f) ZT.

At a Cr doping concentration of 1.5 atm% as shown in Figure 8, the Seebeck coefficient follows a similar trend as in 1 atm% Cr doping (Figure 7) with increasing Se concentration. The peak room-temperature Seebeck coefficient of $-220\ \mu V\ K^{-1}$ was obtained in Te-rich $Cr_{0.015}Pb_{0.985}Te_{0.75}Se_{0.25}$. The electrical conductivity increases when the Se concentration is higher than 50 atm%. The minimum electrical conductivity is observed at equal amount of Te and Se because of the reduction in carrier mobility due to the maximum defect density. As shown in Figure 8, Se-rich samples show higher electrical conductivity but the power factor is not enhanced that much due to the lower Seebeck coefficient. A highest room temperature power factor of $\sim 24\ \mu W\ cm^{-1}\ K^{-2}$ is shown by the Te-rich $Cr_{0.015}Pb_{0.985}Te_{0.75}Se_{0.25}$, which is due to the high value of the Seebeck coefficient and carrier mobility as discussed above. The thermal conductivity is highly reduced due to the alloying effect. A room-temperature thermal conductivity of $\sim 1.2\ W\ m^{-1}\ K^{-1}$ was obtained for the Te-rich sample $Cr_{0.015}Pb_{0.985}Te_{0.75}Se_{0.25}$ and it is a 52% decrease compared to PbTe for the same 1.5 atm% Cr doping level. Thus, by simultaneously reducing the thermal conductivity and enhancing the power factor, a peak ZT of ~ 0.63 is obtained in Te-rich $Cr_{0.015}Pb_{0.985}Te_{0.75}Se_{0.25}$ at room temperature.

The room temperature Pisarenko relation between the Seebeck coefficient and the Hall carrier concentration of $Cr_xPb_{1-x}Te_{1-y}Se_y$ is plotted in Figure 9. All the Hall carrier concentrations are lower than $1.0 \times 10^{19}\ cm^{-3}$ and the absolute Seebeck coefficients are higher than $150\ \mu V\ K^{-1}$ which is more than twice the room temperature Seebeck coefficients of other state-of-the-art p and n-type lead chalcogenide alloy thermoelectric materials $Na_{0.02}Pb_{0.98}Te_{0.75}Se_{0.25}$ [11], $K_{0.02}Pb_{0.98}Te_{0.15}Se_{0.85}$ [20], $In_{0.001}Pb_{0.999}Te_{0.7}Se_{0.3}$ [32], and $PbTe_{0.5}Se_{0.5}$:0.0005 (PbI_2) [33]. The Hall carrier concentration is lower than that of the Cr-doped PbTe if the Se concentration is low (y = 0.25 and 0.5, Te-rich samples), and increases to be higher than that of Cr-doped PbTe with higher Se concentration (y = 0.75 and 1, Se-rich samples). With increasing Hall carrier concentration, the Seebeck coefficient decreases. This fits well with the prediction by the non-parabolic two-band Kane (TBK) model of PbTe and PbSe where acoustic phonon scattering is considered as the dominant carrier scattering mechanisms. From this result the high room temperature Seebeck coefficient is not clearly due to resonance. How does Cr doping affect the band structure needs further study.

From our systematic optimization of the thermoelectric properties of Cr-doped $PbTe_{1-y}Se_y$ by changing Cr concentration or Te:Se ratio, we have identified the best compositions as: $Cr_{0.015}Pb_{0.985}Te_{0.75}Se_{0.25}$ and $Cr_{0.01}Pb_{0.99}Te_{0.25}Se_{0.75}$. Table 1 summarizes the room-temperature properties of these compositions together. The density of both samples is close to their

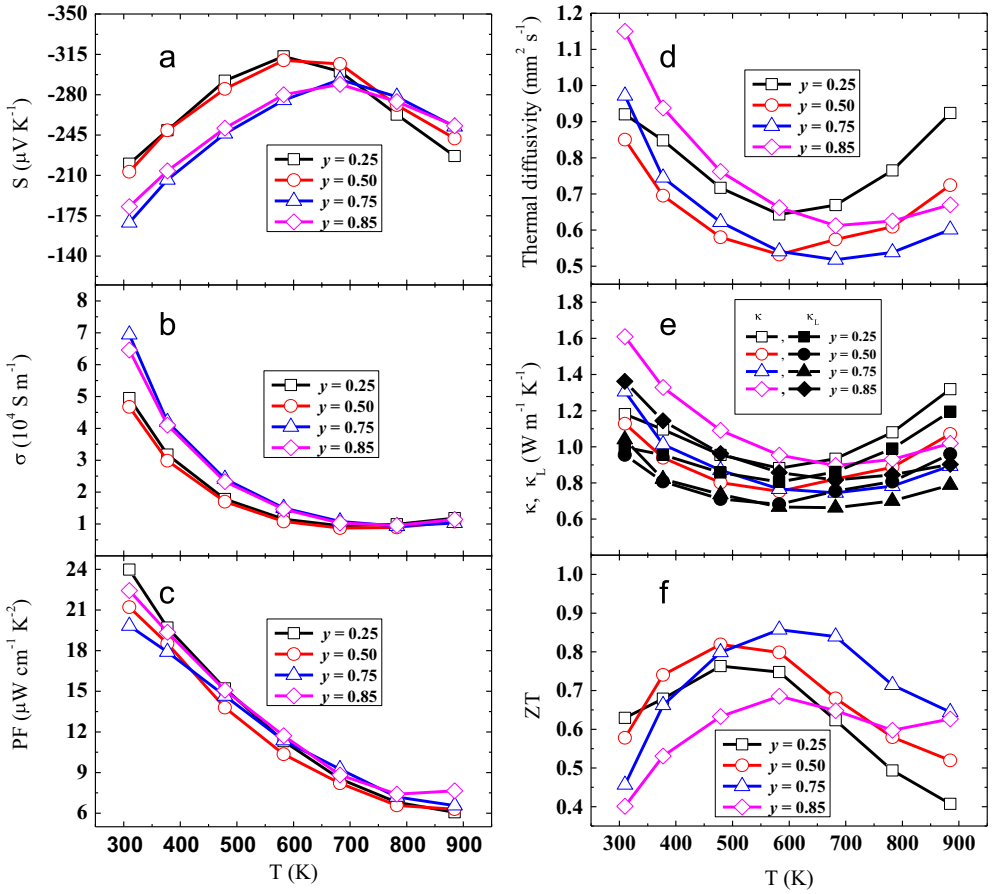

Figure 8 Temperature-dependent thermoelectric properties of $Cr_{0.015}Pb_{0.99}Te_{1-y}Se_y$ (y = 0.25, 0.5, 0.75, and 0.85) with fixed Cr concentration of 1.5 atm%. (a) Seebeck coefficient, (b) electrical conductivity, (c) power factor, (d) thermal diffusivity, (e) total thermal conductivity and lattice thermal conductivity, and (f) ZT.

theoretical density and their carrier concentrations are less than 10^{19} cm^{-3}.

Figure 10 summarizes the effect of Te substitutions by Se on the (a) room-temperature and (b) peak ZTs at fixed Cr doping levels of 1 atm% (black squares) and 1.5 atm% (red circles). As can be seen from the figure, the room-temperature ZT increased when the Se concentration increased up to a certain optimum alloying limit and then decreased when it exceeded this limit. High room-temperature ZTs of ~0.63 and ~0.55 were obtained by substitution of 25 atm% and 75 atm% Te by Se at Cr doping levels of 1.5 atm% and 1 atm%, respectively. As shown in Figures 7 and 8 at fixed Cr concentrations the best peak ZTs are in Se-rich samples. A maximum peak ZT of ~1 is obtained in $Cr_{0.01}Pb_{0.99}Te_{0.25}Se_{0.75}$. The peak ZTs of all the samples are greater than ~0.7 indicating that Cr doping on PbTe alloyed with PbSe brings the best room-temperature thermoelectric properties without or with minimal reduction of the peak ZTs so that the average ZT is improved over the whole temperature range that makes the materials promising for power generation. To show clearly this improvement by Cr doping in $PbTe_{1-y}Se_y$, we also plotted the (a) room temperature power factor, (b) room temperature ZT, and (c) average ZT of $Cr_{0.01}Pb_{0.99}Te_{0.25}Se_{0.75}$ and $Cr_{0.015}Pb_{0.985}Te_{0.75}Se_{0.25}$ as a function of carrier concentration compared with the reported optimized p-type and n-type doped $PbTe_{1-y}Se_y$ in Figure 11. Similar with n-type doped PbSe, [26] both the room temperature power factor and ZT value decreased steeply with the increasing of the room temperature Hall carrier concentration. Although with almost the same carrier concentration, Cr-doped $PbTe_{1-y}Se_y$ has much higher room temperature power factor and ZT value than I-doped $PbTe_{1-y}Se_y$. However, the average ZT is independent on the room temperature carrier concentration. Although with low peak ZT ~1.0 at about 573-673 K, the average ZT of Cr-doped $PbTe_{1-y}Se_y$ is as high as those of p-type $Na_{0.02}Pb_{0.98}Te_{0.75}Se_{0.25}$ (peak ZT ~1.8 at about 850 K) [11] and n-type $PbTe_{0.5}Se_{0.5}$:0.0005 (PbI_2) [33] (peak ZT~1.5 at about 625 K), and higher than those of p-type $K_{0.02}Pb_{0.98}Te_{0.15}Se_{0.85}$ (peak ZT ~1.7 at about 873 K) [20] and n-type $In_{0.001}Pb_{0.999}Te_{0.7}Se_{0.3}$ [32]. The efficiency of thermal to electrical conversion of these selected compositions is discussed in the next section.

The efficiency of a thermoelectric power generator depends on the Carnot efficiency and the thermoelectric figure-of-merit of the devices, which is intrinsic to the materials making up the device. This relation is expressed as follows [34]:

$$\eta_e = \frac{T_h - T_c}{T_h}\left(\frac{\sqrt{1+Z\overline{T}}-1}{\sqrt{1+Z\overline{T}}+(T_c/T_h)}\right) \quad (1)$$

where T_h is the hot-side temperature, T_c is the cold-side temperature, and $\overline{T}$ is the average temperature between T_c

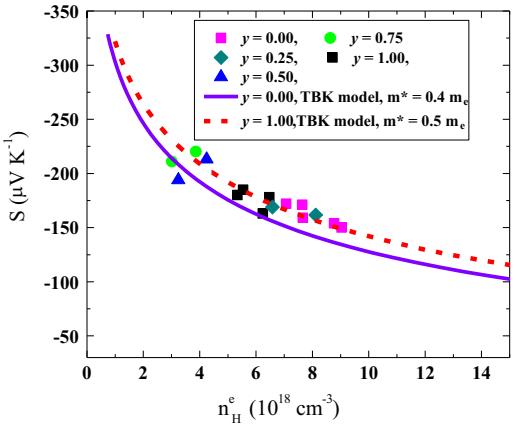

Figure 9 Room-temperature Pisarenko plots of $Cr_xPb_{1-x}Te_{1-y}Se_y$, (■) $Cr_xPb_{1-x}Te$ (x = 0.01, 0.015, 0.025, and 0.03), (●) $Cr_xPb_{1-x}Te_{0.75}Se_{0.25}$ (x = 0.01 and 0.015), (▲) $Cr_xPb_{1-x}Te_{0.5}Se_{0.5}$ (x = 0.01 and 0.015), (◆) $Cr_xPb_{1-x}Te_{0.25}Se_{0.75}$ (x = 0.01 and 0.015), (■) $Cr_xPb_{1-x}Se$ (x = 0.0025, 0.005, 0.0075, 0.01, and 0.02). The purple solid curve is based on a nonparabolic two-band Kane model (TBK) with the electron effective mass of PbTe $m^* = 0.4\ m_e$; the red dashed curve is based on a nonparabolic two-band Kane model (TBK) with the electron effective mass of PbSe $m^* = 0.5\ m_e$.

and T_h. The temperature-dependent properties of the legs are incorporated in the $Z\overline{T}$ term in Eq. (1) and replaced by the average ZT over the whole temperature range when calculating the efficiency. One proposed method of improving the efficiency of thermoelectric generators is designing a segmented device where each segment has a high ZT for the temperature anticipated in the segment [35,36]. However, this technique has its own drawbacks in effectiveness since it suffers from the added complexity of bonding, mass diffusion, and thermal expansion mismatch at the interfaces. Hence, it is important to find a single material with better thermoelectric properties to use over the whole temperature range of operation. Here we propose $Cr_{0.015}Pb_{0.985}Te_{0.75}Se_{0.25}$ and $Cr_{0.01}Pb_{0.99}Te_{0.25}Se_{0.75}$ as potential candidates for a single leg device application to operate from 300 K to 873 K. The leg efficiency can be calculated more accurately by either Snyder or Ursell [37] or Mahan's [35] discretization methods. In this work we used Mahan's method where one dimensional heat flow is assumed in the legs and no heat is lost from the sidewalls. The discretized equations in the leg are given by:

$$\frac{dT}{dx} = \frac{JST - Q}{k} \tag{2}$$

$$\frac{dQ}{dx} = \rho J^2 + JS\frac{dT}{dx} \tag{3}$$

$$\frac{dV}{dx} = -\rho J - S\frac{dT}{dx} \tag{4}$$

where J, Q, ρ, V, S, k and T are the current density, heat flux density, electrical resistivity, voltage, Seebeck coefficient, thermal conductivity, and temperature, respectively. The leg efficiency is calculated from the output power and

Table 1 Room-temperature properties of best optimized Se-rich $Cr_{0.01}Pb_{0.99}Te_{0.25}Se_{0.75}$ and Te-rich $Cr_{0.015}Pb_{0.985}Te_{0.75}Se_{0.25}$ samples.

Nominal Comp.	Real Comp.	Density (g cm^{-3})	S (μV K^{-1})	σ (10^4 S m^{-1})	PF (μW cm^{-1} K^{-2})	κ (W m^{-1} K^{-1})	ZT	n_H (10^{18} cm^{-3})	μ_H (cm^2 V^{-1} s^{-1})
$Cr_{0.01}Pb_{0.99}Te_{0.25}Se_{0.75}$	$Cr_{0.008}Pb_{0.992}Te_{0.21}Se_{0.79}$	7.90	−162	8.29	21.70	1.23	0.54	8.12	638
$Cr_{0.015}Pb_{0.985}Te_{0.75}Se_{0.25}$	$Cr_{0.014}Pb_{0.986}Te_{0.77}Se_{0.23}$	8	−220	6.94	24	1.17	0.63	3.87	1120

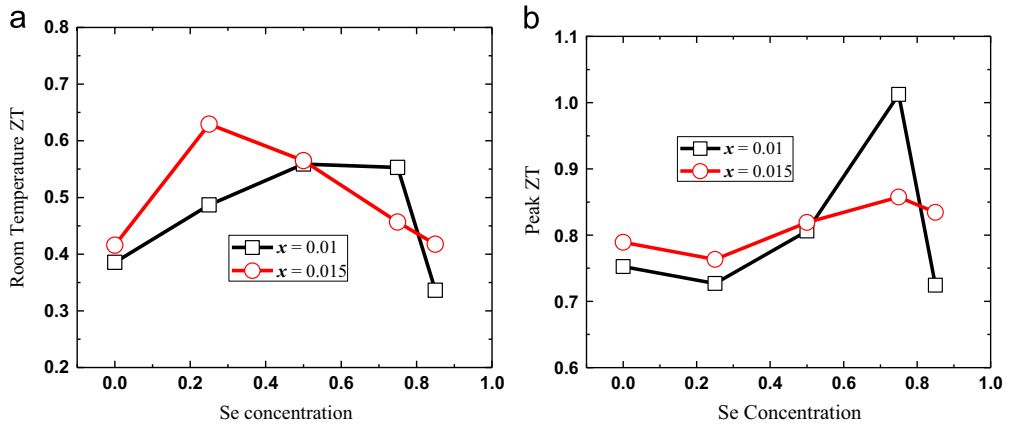

Figure 10 Se concentration dependence of the room temperature *ZT* and peak *ZT* for $Cr_xPb_{1-x}Te_{1-y}$ Se_y.

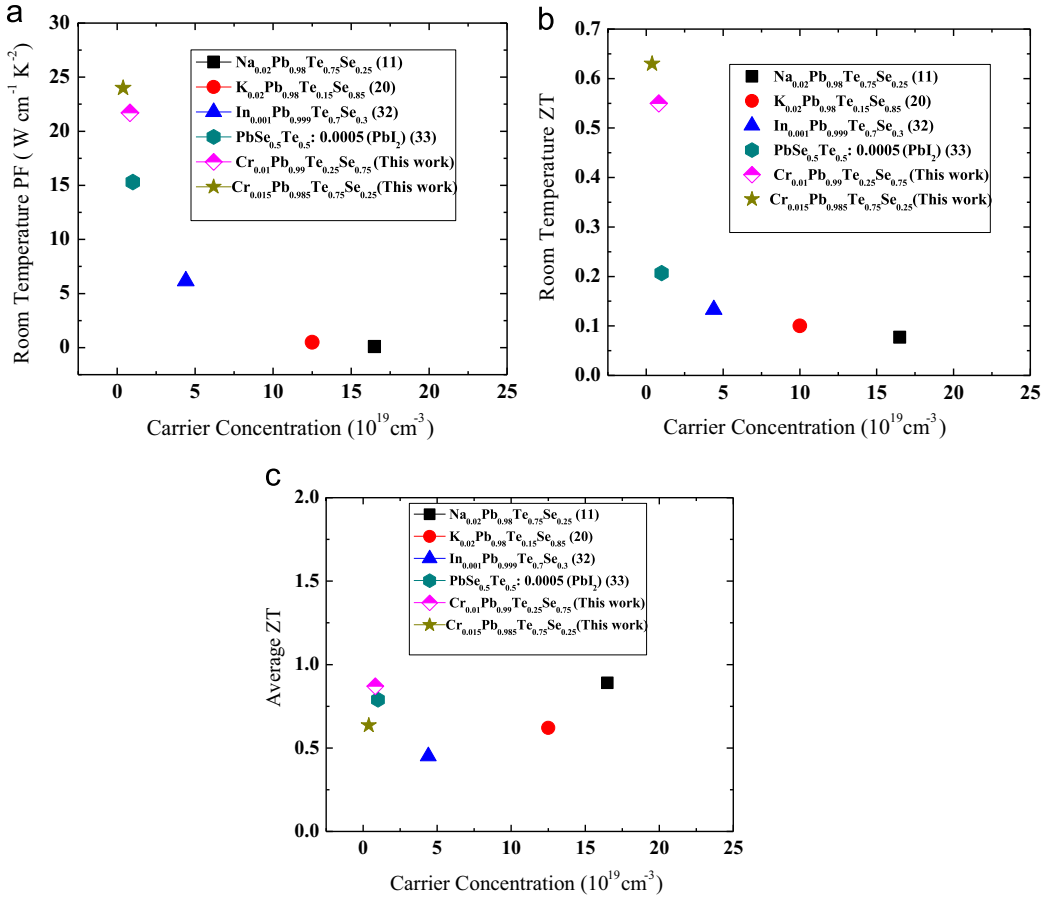

Figure 11 (a) Room temperature power factor, (b) room temperature *ZT*, and (c) average *ZT* of $Cr_{0.01}Pb_{0.99}Te_{0.25}Se_{0.75}$ and $Cr_{0.015}Pb_{0.985}Te_{0.75}Se_{0.25}$ as a function of carrier concentration compared with the reported optimized p-type $Na_{0.02}Pb_{0.98}Te_{0.75}Se_{0.25}$ [11] and $K_{0.02}Pb_{0.98}Te_{0.15}Se_{0.85}$, [20] and n-type $In_{0.001}Pb_{0.999}Te_{0.7}Se_{0.3}$ [32] and $PbSe_{0.5}Te_{0.5}$:0.0005 (PbI_2) [33].

input heat flux into the leg by:

$$\eta_{leg} = \frac{J(V_c - V_h)}{Q_h} \quad (5)$$

The set of coupled first order differential Eqs. (2-4) were iteratively solved with the appropriate temperature boundary conditions at different current densities until the optimum value of *J* that maximizes the leg efficiency is found. We calculated the efficiency of the best compounds, $Cr_{0.015}Pb_{0.985}Te_{0.75}Se_{0.25}$ and $Cr_{0.01}Pb_{0.99}Te_{0.25}Se_{0.75}$, as shown in Figure 12 in comparison with the efficiency of the best optimized Cr-doped PbSe ($Cr_{0.005}Pb_{0.995}Se$), Cr-doped PbTe ($Cr_{0.025}Pb_{0.975}Te$), and I-doped PbTe ($I_{0.0012}PbTe_{0.9988}$). An efficiency of ~11% and ~13% is obtained for the individual legs of $Cr_{0.015}Pb_{0.985}Te_{0.75}Se_{0.25}$ and $Cr_{0.01}Pb_{0.99}Te_{0.25}Se_{0.75}$, respectively, when the cold side temperature is set at 300 K and hot side temperature at 873 K. In spite of having high *ZT* exceeding 1.4 near 700 K for $I_{0.0012}PbTe_{0.9988}$, the efficiency is still lower than that of

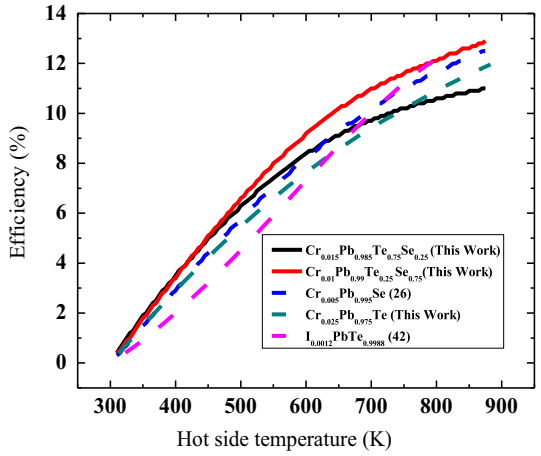

Figure 12 Temperature dependence of the calculated leg efficiencies of $Cr_{0.015}Pb_{0.985}Te_{0.75}Se_{0.25}$ (solid black line), $Cr_{0.01}Pb_{0.99}Te_{0.25}Se_{0.75}$ (solid red line), $Cr_{0.005}Pb_{0.995}Se$ [26] (dashed blue line), $Cr_{0.025}Pb_{0.975}Te$ (dashed green line), and $I_{0.0012}PbTe_{0.9988}$ [42] (dashed pink line) with a cold side temperature at 300 K.

$Cr_{0.01}Pb_{0.99}Te_{0.25}Se_{0.75}$, especially below 700 K. This result is also comparable with the efficiency of other thermoelectric materials with cold side temperature 300 K and hot side temperature 773 K, for example Bi_2Te_3–Bi_2Se_3–Bi_2S_3 (12.5%) [38]. PbSe:Al (9.4%) [15,38] half Heuslers (8.4%) [38,39], filled Skutterrudites (13.1%) [15,40], and PbTe:La (6.7%) [38,41]. This high single leg efficiency over a wide range of temperatures comes from the improvement of the room-temperature *ZT* and then the enhanced average *ZT* over the whole temperature range.

Conclusions

In this systematic study of Cr doping in $PbTe_{1-y}Se_y$, a high figure of merit of ~0.6 at room temperature was achieved in Te-rich $Cr_{0.015}Pb_{0.985}Te_{0.75}Se_{0.25}$ resulting from the combination of a higher power factor and a lower thermal conductivity. A peak *ZT* of ~1 was obtained in Se-rich $Cr_{0.01}Pb_{0.99}Te_{0.25}Se_{0.75}$ at about 573–673 K with a room-temperature *ZT* of ~0.5. The calculated thermal to electrical conversion efficiencies of Te-rich $Cr_{0.015}Pb_{0.985}Te_{0.75}Se_{0.25}$ and Se-rich $Cr_{0.01}Pb_{0.99}Te_{0.25}Se_{0.75}$ are ~11% and ~13%, respectively, with hot side temperature of 873 K and cold side temperature of 300 K and hence could be potentially useful for medium temperature power generation applications.

Acknowledgment

This work is supported by "Solid State Solar Thermal Energy Conversion Center (S^3TEC)", an Energy Frontier Research Center funded by the U.S. Department of Energy, USA Office of Science, USA Office of Basic Energy Science under Award number DE-SC0001299.

Appendix A. Supporting information

Supplementary data associated with this article can be found in the online version at http://dx.doi.org/10.1016/j.nanoen.2015.02.026.

References

[1] G.J. Snyder, E.S. Tobber, Nature Mater. 7 (2008) 105.
[2] Z.G. Chen, G. Han, L. Yang, L. Cheng, J. Zou, Prog. Natural Sci.: Mater. Int. 22 (2012) 535.
[3] T.C. Harman, P.J. Taylor, M.P. Walsh, B.E. Laforge, Science 297 (2002) 2229.
[4] M.S. Dresselhaus, G. Chen, M.Y. Tang, R. Yang, H. Lee, D. Wang, Z.F. Ren, J.P. Fleurial, P. Gogna, Adv. Mater. 19 (2007) 1043.
[5] B.C. Sales, D. Mandrus, R.K. Williams, Science 272 (1996) 1325.
[6] H. Kleinke, Chem. Mater. 22 (2010) 604.
[7] Q. Zhang, T. Sun, F. Cao, M. Li, M.H. Hong, J.K. Yuan, Q.Y. Yan, H.H. Hng, N.Q. Wu, X.G. Liu, Nanoscale 2 (2010) 1256.
[8] W.S. Liu, X. Yan, G. Chen, Z.F. Ren, Nano Energy 1 (2012) 42.
[9] M.S. Dresselhaus, G. Chen, M.Y. Tang, R.G. Yang, H. Lee, D.Z. Wang, Z.F. Ren, J.P. Fleurial, and P. Gogna, Materials and technologies for direct thermal-to-electric energy conversion, in: J. Yang, T.P. Hogan, R. Funahashi, G.S. Nolas (Eds.), Proceedings of the MRS Symposium, Materials Research Society Press, Pittsburgh, PA 2005, pp. 3–12.
[10] M.S. Dresselhaus, J.P. Heremans, in: D.M. Rowe (Ed.), Thermoelectrics Handbook: Macro to Nano, Taylor and Francis, CRC, Boca Raton, FL, 2006, pp. 1–24.
[11] Y. Pei, X. Shi, A. LaLonde, H. Wang, L. Chen, G.J. Snyder, Nature 473 (2011) 66.
[12] S.N. Girard, J. He, X. Zhou, D. Shoemaker, C.M. Jaworski, C. Uher, V.P. Dravid, J.P. Heremans, M.G. Kanatzidis, J. Am. Chem. Soc. 133 (2011) 16588.
[13] Y. Pei, A.D. LaLonde, N.A. Heinz, X. Shi, S. Iwanaga, H. Wang, L. Chen, G.J. Snyder, Adv. Mater. 23 (2011) 5674.
[14] J.P. Heremans, V. Jovovic, E.S. Toberer, A. Saramat, K. Kurosaki, A. Charoenphakdee, S. Yamanaka, G.J. Snyder, Science 321 (2008) 554.
[15] Q.Y. Zhang, H. Wang, W.S. Liu, H.Z. Wang, B. Yu, Q. Zhang, Z.T. Tian, G. Ni, S. Lee, K. Esfarjani, G. Chen, Z.F. Ren, Energy Environ. Sci. 5 (2012) 5246.
[16] J.P. Heremans, B. Wiendlocha, A.M. Chamoire, Energy Environ. Sci. 5 (2012) 5510.
[17] C.M. Jaworski, B. Wiendlocha, V. Jovovic, J.P. Heremans, Energy Environ. Sci. 4 (2011) 4155.
[18] D.M. Rowe, CRC Handbook of Thermoelectrics, CRC Press, Boca Raton London New York Washington, DC, 1995.
[19] A.D. Lalonde, Y. Pei, H. Wang, G.J. Snyder, Mater. Today 14 (2011) 526.
[20] Q. Zhang, F. Cao, W. Liu, K. Lukas, B. Yu, S. Chen, C. Opeil, D. Broido, G. Chen, Z.F. Ren, J. Am. Chem. Soc. 134 (2012) 10031.
[21] B. Basu, S. Bhattacharya, R. Bhatt, A. Singh, D.K. Aswal, S.K. Gupta, J. Electron. Mater. 42 (2013) 2292.
[22] Z.P. Wen, I. Yoshio, I. Yukihiro, S. Yoshikazi, J.X. Peng, Z.G. Tian, Chin. Phys. Lett. 22 (2005) 2103.
[23] P. Zhu, Y. Imai, Y. Isoda, Y. Shinohara, X. Jia, G. Ren, G. Zou, Mater. Trans. 45 (2004) 3102.
[24] E. Grodzicka, W. Dobrowolski, T. Story, A. Wilamowski, and B. Witkowska, The Study of a Resonant Cr Donor in PbTe, PbSe, $PbTe_{1-y}Se_y$ and $Pb_{1-x}Sn_xTe$, Inst. Phys. Conf. Ser. No 144: Section 3 (1995).

[25] B. Paul, P. Banerji, J. Appl. Phys. 109 (2011) 103710.
[26] Q. Zhang, E.K. Chere, K. McEnaney, M.L. Yao, F. Cao, Y.Z. Ni, S. Chen, C. Opeil, G. Chen, Z.F. Ren, Adv. Energy. Mater. (2015). http://dx.doi.org/10.1002/aenm.201401977.
[27] M.D. Nielsen, E.M. Levin, C.M. Jaworski, K. Schmidt-Rohr, J. P. Heremans, Phys. Rev. B 85 (2012) 045210.
[28] D. Parker, D.J. Singh, Phys. Rev B 82 (2010) 035204.
[29] Z. Tian, J. Garg, K. Esfarjani, T. Shiga, J. Shiomi, G. Chen, Phys. Rev. B 85 (2012) 184303.
[30] X. Yan, B. Poudel, Y. Ma, W.S. Liu, G. Joshi, H. Wang, Y. Lan, D. Wang, G. Chen, Z.F. Ren, Nano Lett. 10 (2010) 3373.
[31] H. Wang, Y. Pei, A.D. LaLonde, G.J. Snyder, Proc. Natl. Acad. Sci. USA 109 (25) (2012) 9705–9709.
[32] A. Bali, H. Wang, G.J. Snyder, R.C. Mallik, J. Appl. Phys. 116 (2014) 033707.
[33] P.K. Rawat, B. Paul, P. Banerji, Nanotechnology 24 (2013) 215401.
[34] H.J. Goldsmid, Introduction to Thermoelectricity, Springer-Verlag, Berlin Heidelberg, 2010.
[35] G.D. Mahan, J. Appl. Phys. 70 (1991) 4551.
[36] N.B. Elmer, J. Chin, and G.H. Reynolds, in: Proceedings of the Third International Conference on Thermoelectric Energy Conversion Energy, (Ed.) K. R. Rao, Arlington, TX, (IEEE, New York, 1980), p. 105.
[37] G.J. Snyder, T.S. Ursell, Phys. Rev. Lett. 91 (2003) 148301.
[38] W.S. Liu, K.C. Lukas, K.M. Enaney, S. Lee, Q. Zhang, C. Opeil, G. Chen, Z.F. Ren, Energy Environ. Sci. 6 (2013) 552.
[39] G. Joshi, X. Yan, H.Z. Wang, W.S. Liu, G. Chen, Z.F. Ren, Adv. Energy Mater. 1 (2011) 643.
[40] X. Shi, J. Yang, J.R. Salvador, M.F. Chi, J.Y. Cho, H. Wang, S.Q. Bai, J.H. Yang, W.Q. Zhang, L.D. Chen, J. Am. Chem. Soc. 133 (2011) 7837.
[41] Y.Z. Pei, J. Lensch-Falk, E.S. Toberer, D.L. Medlin, G.J. Snyder, Adv. Funct. Mater. 21 (2011) 241.
[42] A.D. LaLonde, Y. Pei, G.J. Snyder, Energy Environ. Sci. 4 (2011) 2090.

Eyob K. Chere is currently a Ph.D. student at the University of Houston department of Physics, Houston, Texas USA. He got his B. Sc. in Physics from Bahirdar University, Ethiopia in 2006, his M.sc. in Materials Science from Addis Ababa University, Ethiopia in 2010, and postgraduate diploma in condensed matter physics from the international center for theoretical physics (ICTP), Trieste, Italy in 2011. He is currently working on improving the thermoelectric performance of group IV–VI alloys and discovering new potential thermoelectric IV–VI compounds.

Qian Zhang, Ph.D., is currently a Research Associate in the Department of Physics and TcSUH at the University of Houston, USA. She received her Ph.D. degree in Materials Science and Engineering from Zhejiang University, China. She completed her doctoral thesis from 2006 to 2009 for the research of Mg2(Si,Sn) based thermoelectric materials. Her current research is mainly on enhancing the existing and discovering new group IV–VI thermoelectric materials.

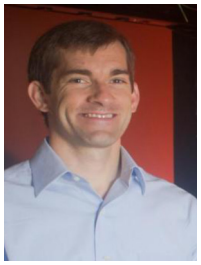

Kenneth McEnaney is an engineer at Creare, an engineering R&D company based on Hanover, New Hampshire. He earned his Ph.D. in Mechanical Engineering from MIT in 2014. His research focused on segmented thermoelectric generators, solar thermoelectric generators, and heat transfer in aerogels. Prior to MIT, Ken earned his B.S. in Mechanical Engineering from Cornell University in 2002 and worked as a senior engineer at Boston Flight Sciences.

Mengliang Yao has been a Ph.D. candidate at Boston College since 2010. He received his B.S. degree and M.S. degree in the Department of Physics from Nanjing University in 2007 and 2010, respectively. His current research is mainly on transport measurements in thermoelectric materials.

Feng Cao, Ph.D., is currently a Research Associate in the Department of Physics and TcSUH at the University of Houston, USA. He received his Ph.D. degree in Physics from the Hong Kong Polytechnic University in 2012. His current research is mainly focused on the optimization and designing of solar selective coatings for harvesting solar radiation.

Jingying Sun is currently a second year graduate student in the Department of Physics and TcSUH at the University of Houston. She received her B.S. degree in Physics from Jilin University, China. Her current research is mainly on lithium-ion battery and in-situ transmission electron microscope.

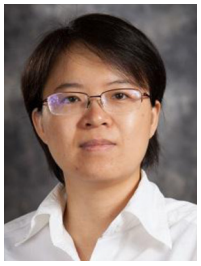

Dr. Shuo Chen is currently an Assistant Professor in the Department of Physics and the Texas Center for Superconductivity at the University of Houston. She earned her BS degree in Physics at Peking University, China and a Ph.D. degree from the Department of Physics at Boston College. Her research interests cover the material/device fabrication for clean/green energy application purposes and in situ Transmission Electron Microscopy.

Cyril P. Opeil, S.J., is currently an Assistant Professor of Physics at Boston College. He specializes in low-temperature thermodynamic measurements. His research interests include martinsite alloys, ferroelectric materials, thermoelectrics and the formation of meteorites.

Dr. Gang Chen is currently the Carl Richard Soderberg Professor of Power Engineering at Massachusetts Institute of Technology. He obtained his Ph.D. degree from UC Berkeley in 1993 working under then Chancellor Chang-Lin Tien, Master and Bachelor degrees from Huazhong University of Science and Technology, China. He was a faculty member at Duke University (1993–1997), University of California at Los Angeles (1997–2001), before joining MIT in 2001. He is a member of national Academy of Engineering. He is a recipient of the NSF Young Investigator Award, the ASME Heat Transfer Memorial Award, and the R&D100 Award. He is a Guggenheim Fellow, an AAAS Fellow, an ASME Fellow, and an APS Fellow. He has published extensively in the area of nanoscale energy transport and conversion and nanoscale heat transfer. He is the director of Solid-State Solar-Thermal Energy Conversion Center funded by the US DOE's Energy Frontier Research Centers program."

Dr. Zhifeng Ren is currently an M.D. Anderson Chair Professor in the Department of Physics and TcSUH at the University of Houston. He obtained his Ph.D. degree from the Institute of Physics Chinese Academy of Sciences in 1990, master degree from Huazhong University of Science and Technology in 1987, and bachelor degree from Sichuan Institute of Technology in 1984. He was a postdoc and research faculty at SUNY Buffalo (1990–1999) before joining BC in 1999. He specializes in thermoelectric materials, solar thermoelectric devices & systems, flexible transparent conductors, photovoltaic materials, carbon nanotubes & semiconducting nanostructures, bio agent delivery & bio sensors, superconductors, etc. He is a fellow of APS, AAA and NAI, a recipient of R&D 100 award and the 2014 O'Donnell award in Science of TAMEST. He has published 340 papers.